Optical phased array using high contrast gratings for two dimensional beamforming and beamsteering

Byung-Wook Yoo,[1,*] Mischa Megens,[1,2] Trevor Chan,[2] Tianbo Sun,[1] Weijian Yang,[1] Connie J. Chang-Hasnain,[1] David A. Horsley,[2] and Ming C. Wu[1]

[1]*School of Electrical Engineering and Computer Sciences, University of California Berkeley, Berkeley, CA, 94720, USA*

[2]*Department of Mechanical and Aerospace Engineering, University of California Davis, Davis, CA, 95616, USA*

[*]*yoo@eecs.berkeley.edu*

Abstract: We have developed a microelectromechanical system (MEMS) optical phased array incorporating a high-index-contrast subwavelength grating (HCG) for beamforming and beamsteering in a range of ± 1.26° × 1.26°. Our approach needs only a thin single-layer HCG made of silicon, considerably improving its speed thanks to the low mass, and is suitable for high optical power applications. The measured resonant frequency of HCG is 0.32 MHz.

OCIS codes: (110.5100) Phased-array imaging systems; (230.1950) Diffraction gratings; (230.3990) Micro-optical devices.

References and links

1. P. F. McManamon, P. J. Bos, M. J. Escuti, J. Heikenfeld, S. Serati, H. Xie, and E. A. Watson, "A review of phased array steering for narrow-band electrooptical systems," Proc. IEEE **97**(6), 1078–1096 (2009).
2. B. Wang, G. Zhang, A. Glushchenko, J. L. West, P. J. Bos, and P. F. McManamon, "Stressed liquid-crystal optical phased array for fast tip-tilt wavefront correction," Appl. Opt. **44**(36), 7754–7759 (2005).
3. H. C. Jau, T. H. Lin, R. X. Fung, S. Y. Huang, J. H. Liu, and A. Y. Fuh, "Optically-tunable beam steering grating based n azobenzene doped cholesteric liquid crystal," Opt. Express **18**(16), 17498–17503 (2010).
4. D. Engström, M. J. O'Callaghan, C. Walker, and M. A. Handschy, "Fast beam steering with a ferroelectric-liquid-crystal optical phased array," Appl. Opt. **48**(9), 1721–1726 (2009).
5. O. Solgaard, F. S. A. Sandejas, and D. M. Bloom, "Deformable grating optical modulator," Opt. Lett. **17**(9), 688–690 (1992).
6. S. Senturia, "Programmable diffraction gratings and their uses in displays, spectroscopy, and communications," Proc. SPIE **5348**, 1–6 (2004).
7. U. Krishnamoorthy, K. Li, K. Yu, D. Lee, J. P. Heritage, and O. Solgaard, "Dual-mode micromirrors for optical phased array applications," Sens. Actua. A **97–98**, 21–26 (2002).
8. K. H. Koh and C. Lee, "A two-dimensional MEMS scanning mirror using hybrid actuation mechanisms with low operation voltage," J. Microelectromech. Syst. **21**(5), 1124–1135 (2012).
9. M. C. Y. Huang, Y. Zhou, and C. J. Chang-Hasnain, "A surface-emitting laser incorporating a high-index-contrast subwavelength grating," Nat. Photonics **1**(2), 119–122 (2007).
10. C. F. R. Mateus, M. C. Y. Huang, Y. Deng, A. Neureuther, and C. J. Chang-Hasnain, "Ultrabroadband mirror using low-index cladded subwavelength grating," IEEE Photon. Technol. Lett. **16**, 518–520 (2004).
11. V. Karagodsky and C. J. Chang-Hasnain, "Physics of near-wavelength high contrast gratings," Opt. Express **20**, 10888–10895 (2012).
12. C. J. Chang-Hasnain and W. Yang, "High-contrast gratings for integrated optoelectronics," Adv. Opt. Photon. **4**(3), 379–440 (2012).
13. F. Tounsi, L. Rufer, B. Mezghani, M. Masmoudi, and S. Mir, "Highly flexible membrane systems for micromachined microphones – modeling and simulation," International Conference on Signals, Circuits and Systems, 1–6 (2009).
14. C. Knoernschild, C. Kim, C. W. Gregory, F. P. Lu, and J. Kim, "Investigation of optical power tolerance for MEMS mirrors," J. Microelectromech. Syst. **19**(3), 640–646 (2010).
15. T. K. Chan, M. Megens, B. W. Yoo, J. Wyras, C. J. Chang-Hasnain, M. C. Wu, and D. A. Horsley, "Optical beamsteering using an 8 × 8 MEMS phased array with closed-loop interferometric phase control," Opt. Express **21**(3), 2807–2815 (2013).
16. B. Bhushan, *Springer handbook of nanotechnology* (Springer, 2010), Part F.

#182670 - $15.00 USD Received 2 Jan 2013; revised 8 Mar 2013; accepted 13 Mar 2013; published 10 May 2013

1. Introduction

Optical phased arrays (OPA) have generated a growing interest in many application areas regarding beamforming and beamsteering [1]. For example, laser radar is one of the most attention-grabbing applications for target detection, surveying and mapping, and gas cloud identification. Free space optical communication also benefits from the current technologies realizing directed beams with encoded information in free space. Phased arrays able to handle very high power direct lasers can potentially enable missile defense shield systems, if the speed of beamsteering is sufficiently fast.

For the implementation of fast beamsteering using phased arrays, there have been many research efforts in the last two decades. The most common approach to phased arrays is liquid crystal based [2]. A liquid crystal phased array is comparatively easy to construct and its driving voltage is low. Among many liquid crystal approaches, nematic-phase liquid crystals provide a practical implementation of high-performance phased arrays, however, most of these have limited steering angle, slow switching speed (tens of milliseconds) and suffer from dispersion. For example, H. C. Jau implemented optically tunable beamsteering with an angular range of ~19 degrees using azobenzene doped cholesteric liquid crystals, but the tuning required a few seconds to complete [3]. Attempts to overcome these switching speed limitations have been made by D. Engström working on fast beamsteering using ferroelectric liquid crystal phased arrays. However the rise/fall times were still in the range 140-180 μs, limiting the application area [4].

In recent years, MEMS technology for beamsteering has emerged to offer several advantages such as fast operating speed, low energy consumption and high optical efficiency [5–8]. D. M. Bloom introduced the Grating Light Valve^{TM} technology using micromechanical phase gratings for display, showing 1 μs response time and high contrast ratio [5]. Polychromix used the same basic architecture as the Grating Light Valve with a longer ribbon for low price spectrometers [6]. In general, however, MEMS mirrors need a reflective coating on top of actuator, resulting in limited capability for high optical power density applications.

In this paper, we present a MEMS high contrast grating (HCG) phased array for very fast beamsteering using an array of small aperture MEMS mirrors incorporating a single silicon layer HCG reflector as shown in Fig. 1. The thin and lightweight single layer of small subaperture mirrors is not only suitable for fast time response on the order of microseconds with low voltage actuation, but is also capable of handling high optical power.

2. Design

2.1 The principle of MEMS HCG optical phased arrays

The principle of MEMS phased arrays for beamsteering is schematically depicted in Fig. 1. Light is normally incident on the 8 × 8 array of HCG mirrors that are electrostatically actuated toward the substrate in a piston fashion. The light is reflected back and its phase (φ) is modulated to alter the shape of the reflected light wavefront. This phase modulation enables not only to steer the propagation direction of the light by using a modulo 2π steering approach, but also to focus by imparting a parabolic phase profile [1].

#182670 - $15.00 USD Received 2 Jan 2013; revised 8 Mar 2013; accepted 13 Mar 2013; published 10 May 2013

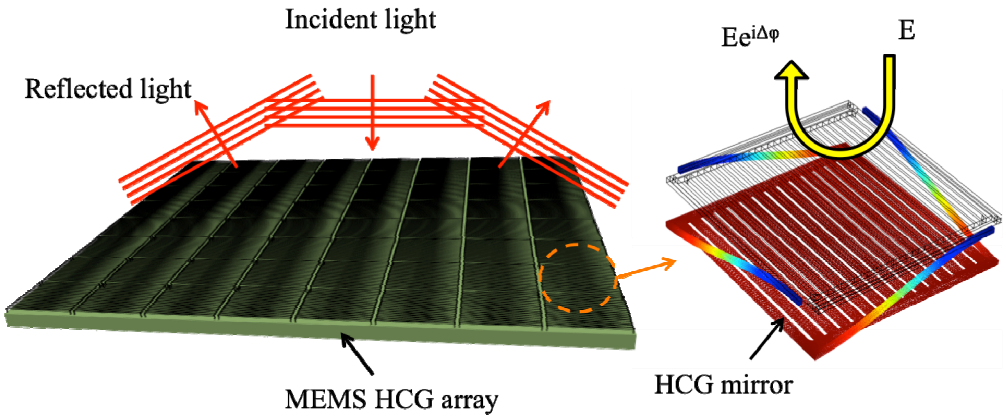

Fig. 1. Schematic view of MEMS phased array composed of high contrast grating mirrors.

The HCG is made of single crystal silicon without metal coating. HCG mirrors are much faster than any other single-aperture MEMS mirror for the purpose of beamsteering because they have much lower mass and inertia. Moreover, OPAs incorporating sub-wavelength gratings have significant advantages over conventional MEMS phased arrays, using only a single material with wide applicability in high power laser system.

In particular, HCGs have become a subject of special interest regarding their very high reflectivity along a broad bandwidth, wider than distributed Bragg reflectors (DBR), as illustrated in Fig. 2. The HCG and DBR in Fig. 2 are both designed to reach 99.9% reflectivity at 1550 nm. The dimensions of HCG are chosen so that it has 99.9% reflectivity for transverse-electric (TE)-polarized light of 1550 nm wavelength via extensive investigations on the duty cycle and thickness of gratings using the rigorous coupled wave analysis (RCWA) method. The high reflectivity of HCGs has been demonstrated both experimentally and theoretically by Chang-Hasnain [9–12]. The physical mechanism behind the high reflectivity of HCG is shown in the inset of Fig. 2. The incident light excites multiple (typically two) optical modes within the HCG. As these modes reach the bottom of the HCG, they interfere destructively, which prevents the transmitted wave from being launched, thus resulting in ~100% of the power to be reflected. A reflectivity higher than 99% can be maintained over a broad wavelength range of $\Delta\lambda/\lambda$~30% as reported in [10]. For comparison: a reflectivity as high as 99% for a DBR typically requires 20 to 40 pairs of alternating index materials, resulting in ~100 times heavier reflector than an HCG [11, 12]. Because of its low mass, the HCG has advantages as a very fast MEMS mirror.

#182670 - $15.00 USD Received 2 Jan 2013; revised 8 Mar 2013; accepted 13 Mar 2013; published 10 May 2013

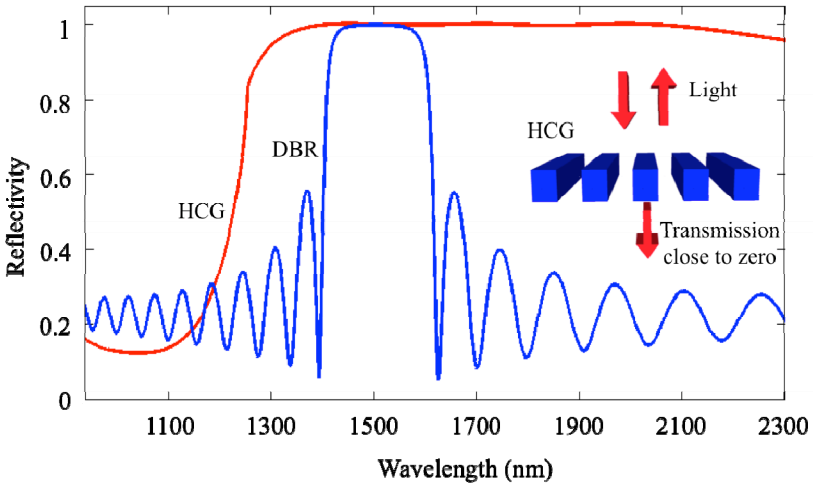

Fig. 2. Reflectance spectrum of an HCG compared to a DBR. The inset illustrates the simplified principle of reflection.

2.2 The design of MEMS HCGs

The specific design of the HCG for our MEMS phased array is as follows: period = 1380 nm, width = 670 nm and thickness = 320 nm. The mirror, 20 × 20 μm^2, is tethered to four anchors with four springs. The width (w) and thickness (t) of the springs are designed to be 350 nm and 320 nm, respectively. The lengths of the two beam segments in each spring are 18.7 μm (L_b) and 700 nm (L_a). The HCG mirror features resonance in the z direction at a frequency

$$f_z = \frac{1}{2\pi}\sqrt{\frac{k}{m}}. \tag{1}$$

where k and m represent the spring constant and the HCG mirror mass, respectively. For the crab-leg spring design, the spring constant can be calculated by using the equation in [13]. Since the length of the spring (L_b), 18.7 μm, is much longer than the other segment of the spring (L_a), 700 nm, k can be simplified to be

$$k = \frac{4Ewt^3}{L_b^3}. \tag{2}$$

With the fixed spring constant based on the dimensions above and Young's modulus (E = 169 GPa), k = 1.185 N/m, the lightweight grating structure can be designed to attain a resonant frequency of 463 kHz thanks to its low mass, 139 pg. The calculation result is confirmed with the Finite Element Method (FEM) simulation result using COMSOL software, 443 kHz, as shown in Fig. 3(a). Figure 3(b) describes that lighter weight structures have a higher resonant frequency. Because MEMS devices with higher resonant frequency show a faster transient response, MEMS designs with high resonant frequency are typically preferable as OPAs for beamsteering applications. As HCG mirrors are thousands of times lighter than conventional MEMS beam scanners and DBR mirrors, OPAs incorporating HCGs are especially suitable for fast beamsteering.

#182670 - $15.00 USD Received 2 Jan 2013; revised 8 Mar 2013; accepted 13 Mar 2013; published 10 May 2013

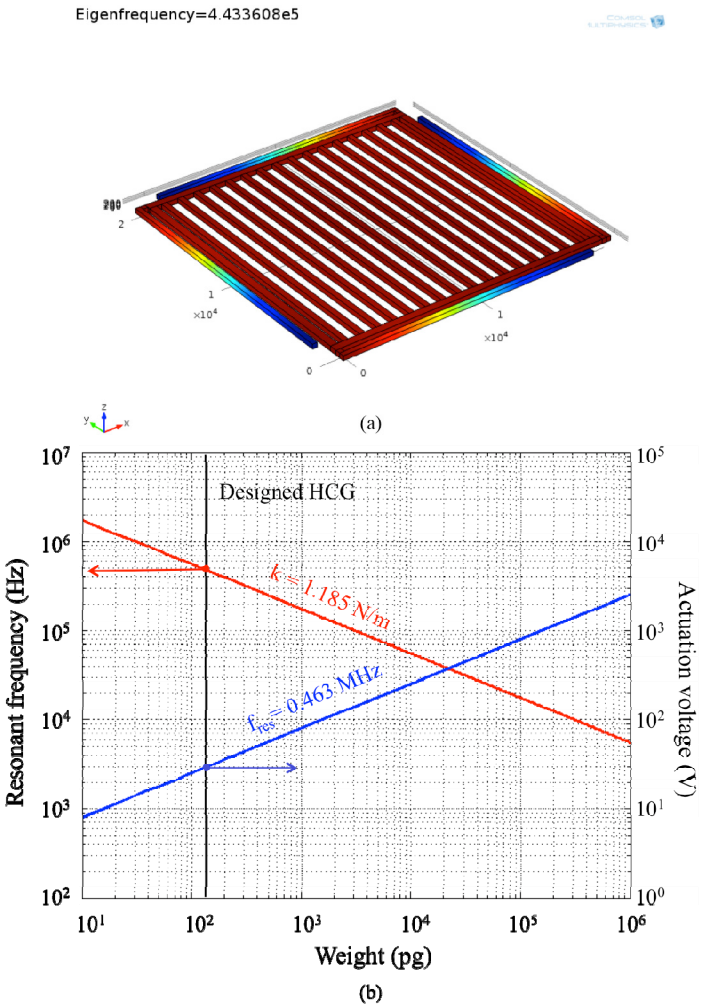

Fig. 3. (a) Modal analysis using COMSOL software showing the 1st resonance mode at 443 kHz, (b) At a fixed resonant frequency (blue curve), low mass reduces the required voltage to generate 775 nm actuation range (corresponding to 2π phase shift at the wavelength of 1550 nm); at fixed spring constant (red curve), low mass increases the speed of the device.

For low voltage actuation with fixed resonant frequency, the light weight of a HCG is also of benefit. For a fixed resonant frequency in Eq. (1), a lightweight HCG mirror can use a lower spring constant k than traditional mirrors. The total potential energy in the system is:

$$U = -\frac{1}{2}\frac{\varepsilon A}{g-x}V^2 + \frac{1}{2}kx^2. \tag{3}$$

where ε is the air permittivity, A is the area of the mirror, V is the applied voltage, g is the initial actuation gap and x is the mirror displacement. The first term is the electrostatic potential of the mirror and the second term is the mechanical energy stored in the cantilever springs. The force acting on the movable mirror is obtained by taking the derivative of Eq. (3) with respect to x. The equilibrium of electrostatic force and spring force provides:

$$V = \sqrt{\frac{2kx}{\varepsilon A}}(g-x). \tag{4}$$

#182670 - $15.00 USD Received 2 Jan 2013; revised 8 Mar 2013; accepted 13 Mar 2013; published 10 May 2013

In Eq. (4), the actuation voltage of the HCG mirror is shown to become lower thanks to the lower spring constant obtained from its light weight compared with traditional mirrors. For example, the required snap-down voltage of the HCG is less than 30 V. In Fig. 3, the snap-down voltage for a 1000 times heavier device with the same resonant frequency is close to 1000 V, which is impractical, especially when a MEMS device is operated in air.

HCG mirrors comprise a single layer of silicon. This feature enables HCG mirrors to be free from thermal induced stress as well as initial deformation from residual stress. In contrast, conventional MEMS mirrors are coated with metal to provide high reflectance. During the heating from a light source, such MEMS mirrors become distorted due to the stress caused by temperature change and different coefficients of thermal expansion of the mirror materials. Once MEMS mirrors become warped from the heating, they distort the wavefront. For example, a polysilicon mirror plate expands less than the reflective metal coating on top due to the mismatch in their coefficients of thermal expansion. Knoernschild and Kim experimentally demonstrated the flatness variation of gold-coated and aluminum-coated MEMS silicon mirrors, which are heated with high optical power [14]. Based on the criteria of a surface flatness of $\lambda/20$ for precision optics, a gold-coated mirror can tolerate only 1.27 W/mm^2 of optical power at the 532 nm wavelength and an aluminum-coated mirror can handle 3.98 W/mm^2 at the same wavelength, because of the mirror heating. The HCG, on the other hand, is composed only of a single layer of silicon. By achieving high reflectivity in HCG design and high fill-factor in the OPA design, mirror deformation from high energy lasers may not be an issue. Then, HCGs can remain consistently flatter than conventional MEMS mirrors at high temperatures caused by high power lasers.

3. Fabrication

Our optical phased arrays are fabricated using a SOI wafer with 320 nm-thick device layer and 2 μm-thick buried oxide (BOX) layer. Only one photolithography mask is used in the fabrication process, resulting in easy fabrication, high yield and low cost. After a standard cleaning process with sulfuric peroxide mixture and buffered hydrofluoric (HF) acid, the device layer of a SOI wafer is heavily doped using solid boron in a furnace to be 23 **Ω**/sq, providing electrical lines of low electrical resistance. Using a deep ultraviolet (DUV) ASML300 stepper, the top silicon layer of the SOI wafer is patterned with the phased array. Then, anisotropic dry etching follows and HF vapor etching is used to remove the BOX layer, releasing the HCGs. The HF vapor etching process requires anchors that are large enough to have some BOX layer remain underneath while the 2 μm-thick BOX layer under the HCGs is totally removed and the HCGs are released. However, large anchors will reduce the maximum beamsteering angle imposed by the mirror pitch. Therefore, two separate anisotropic dry etching steps are applied, one for the device layer and another for the partial BOX layer. First, dry etching of silicon is performed to define 320 nm-deep OPA patterns on the device layer using Cl_2 and HBr. Second, an anisotropic dry etching using CF_4 follows to partially etch the BOX layer in the vertical direction to shorten the release process time of isotropic etching using HF vapor. With only the isotropic HF vapor etching, very large anchors would be required to be able to survive until the silicon ground plane is revealed, resulting in low fill-factor.

#182670 - $15.00 USD Received 2 Jan 2013; revised 8 Mar 2013; accepted 13 Mar 2013; published 10 May 2013

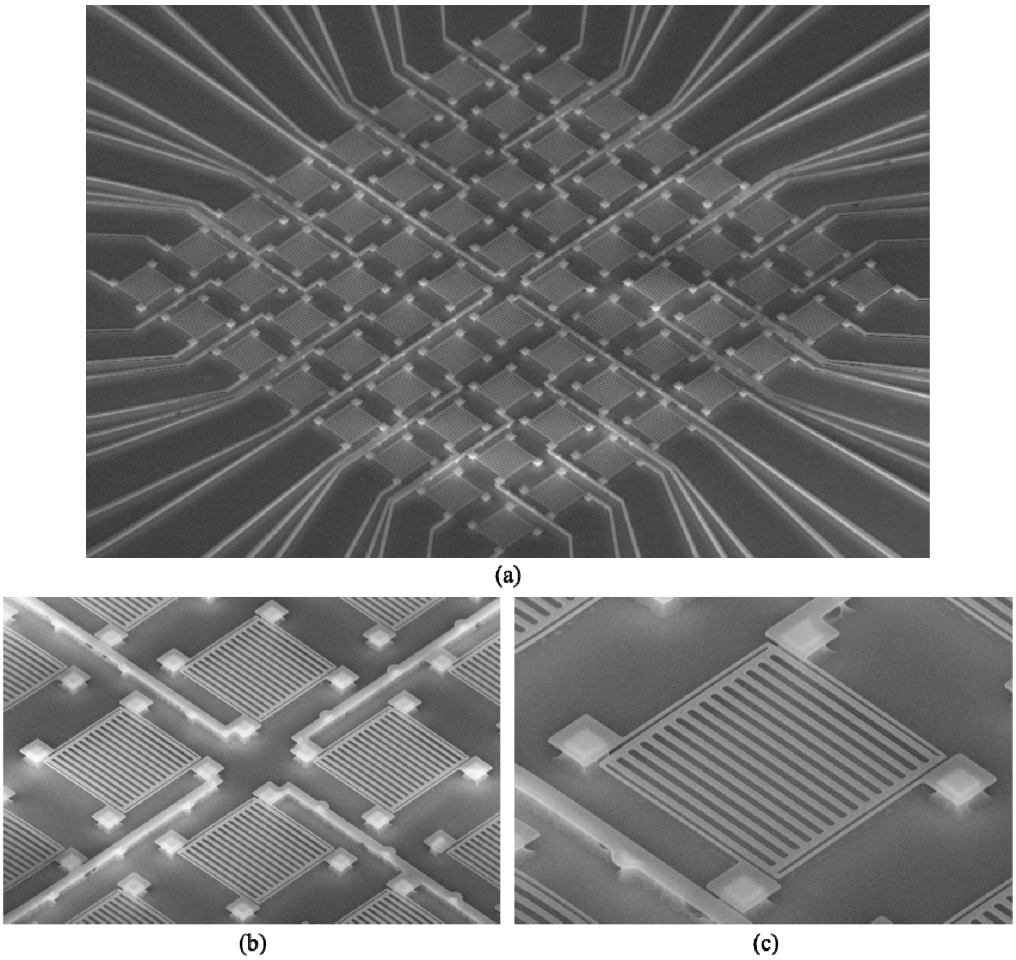

Fig. 4. SEM images of the fabricated OPA. (a) 8 × 8 MEMS HCG array, (b) four HCG mirrors and electrical lines connected via the anchors, (c) HCG mirror with four mechanical springs showing remaining BOX layer beneath each of the four anchors.

Figure 4(a) shows the fabrication result of a phased array composed of 64 HCG mirrors. The electrical addressing lines are designed to be wide enough not to be released during HF vapor etching. Anchors are sufficiently large for the same reason. The pitch of the OPA is designed to be 35 μm, resulting in 36% fill-factor. Figures 4(b)-4(c) show enlarged views of individual mirrors, showing the delicate thin grating bars of the HCGs. The oxide undercuts can be seen through the thin silicon device layer. When the oxide undercut is too great, the 2 μm wide electrical lines are not supported by the BOX layer. When applying voltage to these over-etched samples, some electrical lines snap into contact with the grounded substrate, leading to a short circuit. Therefore, sufficient anisotropic dry etching of oxide is required prior to HF vapor release. However, the dry etch has relatively low selectivity between oxide and silicon, resulting in thinned and narrowed silicon springs due to the large openings around the HCG. As a result, the spring constant becomes lower than designed. We measured resonant frequencies using a commercial laser Doppler vibrometer (LDV) system. The average resonant frequency of the phased array is measured to be 317.15 kHz in Fig. 5. Its standard deviation is 5.93 kHz, equivalent to 1.8%. Thanks to the high uniformity of the measured HCGs, the actuation voltage is expected to be uniform as well, based on Eq. (1) and Eq. (4).

#182670 - $15.00 USD Received 2 Jan 2013; revised 8 Mar 2013; accepted 13 Mar 2013; published 10 May 2013

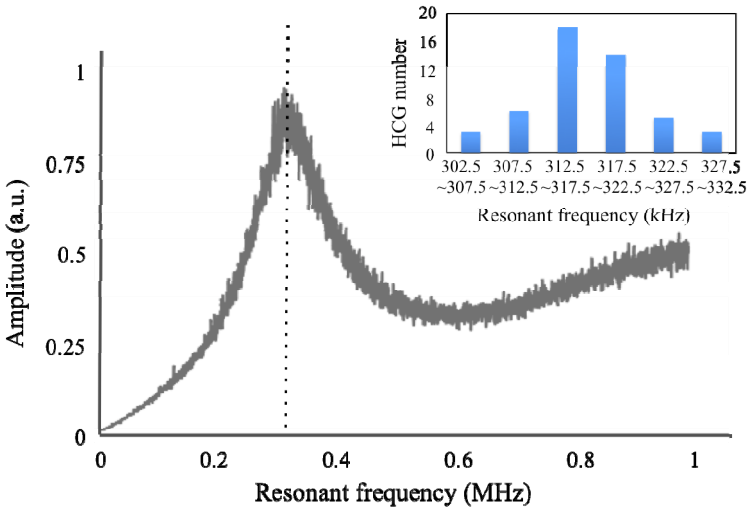

Fig. 5. Experimental resonant frequency of an HCG. The inset shows a histogram of the resonant frequency measured over the 8 × 8 array, demonstrating 1.8% uniformity.

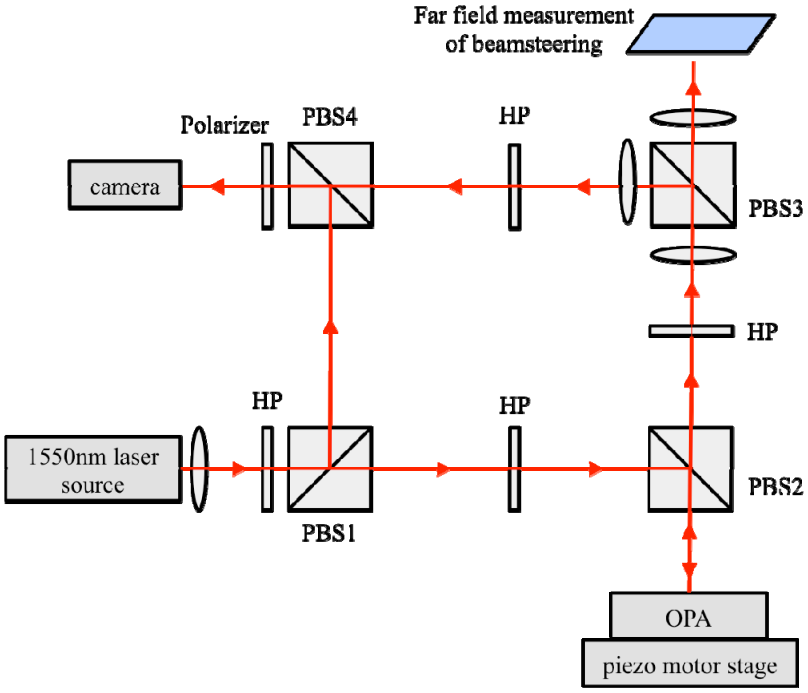

Fig. 6. Optical set-up for in situ stroboscopic interferometric imaging.

4. Experimental results

It is essential to have precise imaging and phase shift control of the HCG array for accurate and fast beamsteering. Figure 6 shows our experiment set-up for in situ stroboscopic interferometric imaging. This set-up is composed of a 1550 nm laser source, polarizing beam splitter cubes (PBS), half-wave plates (HP), and lenses. The reference beam is split from the laser source by PBS1 toward PBS4, while most of the power is transferred from PBS1 to PBS2 and on to the phased array. The light is normally incident on the phased array, which is

#182670 - $15.00 USD Received 2 Jan 2013; revised 8 Mar 2013; accepted 13 Mar 2013; published 10 May 2013

oriented with its grating bars at 45° with respect to the beam polarization. Part of the reflected beam passes through PBS2, and its polarization is rotated by a HP so as to allocate most of the power for the steered output through PBS3. The remaining beam is combined with a reference beam to form an interference pattern, which is sampled by a camera. The interferometer path length is changed using a piezo to resolve the phase shift modulo 2π of each mirror. Two sets of lenses (AC080-010-C and AC254-75-C from Thorlabs) help relay an image of the phased array to the camera and magnify the field of view of the beamsteering [15].

We measured the time response of the HCG, shown in Fig. 7, with the interferometer. A 20-μs-long voltage pulse is applied to the HCG, resulting in a displacement of the mirror and a shift in optical phase. The mirror exhibits ringing after each transition. The motion is fitted to a damped harmonic oscillator model in Fig. 7. The frequency and damping of the ringing is different after switching on or off. This difference is caused by the change in resonant frequency of the electrostatically-actuated MEMS HCG when the voltage varies, because its effective spring constant depends on the applied voltage. Based on the fitted curve, the frequency of oscillation after transition from the on state to the off state is 314 kHz ($1/f = 3.18$ μs), which is in good agreement with the measured resonant frequency of the MEMS HCG, 317.15 kHz, in Fig. 5. The frequency of the ringing after transition from the off state to the on state is 171 kHz ($1/f = 5.83$ μs), implying that effective spring constant decreases when the voltage is on, because the electrostatic spring constant acts as a negative spring during the electrostatic microactuator operation [16]. The motion is almost critically damped, even at this high frequency, without vacuum packaging.

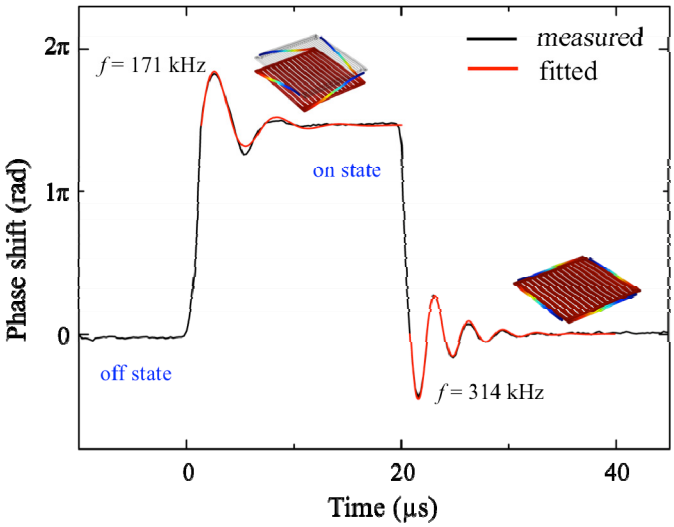

Fig. 7. Comparison of measured time response and damped harmonic oscillator fitting

The beamsteering angle is measured in the experiment set-up of Fig. 6. For a normally incident beam, the beamsteering angle is expected to be

$$\sin\theta = \pm\frac{\lambda}{2\Lambda}. \tag{5}$$

where λ is the design wavelength for the phased array, 1550 nm, and Λ is the mirror pitch, 35 μm. The maximum steering angle is expected to be ± 1.26°. The total field of view is magnified to ~ ± 10° via a pair of achromatic doublet lenses. Figure 8(a) shows a quadrant of the optical output from the phased array when no voltage is applied. The unbiased phased array provides a strong zeroth order beam and grating sidelobes in both x and y directions in

#182670 - $15.00 USD Received 2 Jan 2013; revised 8 Mar 2013; accepted 13 Mar 2013; published 10 May 2013

Fig. 8(a). Figure 8(b) depicts a quadrant of the optical output of the maximum beamsteering angle along the horizontal axis. As is shown in the inset of Fig. 8(b), 18 V is applied to every other column to achieve 0 and π phase shift in alternating columns in the phase map. Figure 8(c) presents the maximum beamsteering angle along the vertical axis using the phase map in the inset. Cross-sectional views of the camera images are converted to the graphs in Figs. 8 (d)-8(e). The noise in the signal outside the peaks is mostly caused by low fill-factor and all features between the HCGs such as anchoring posts and electrical lines. This can be improved by increasing the fill-factor of the phased array. The measured beamsteering angles and widths match very well with the theoretical predictions. In Figs. 8(d)-8(e), the ratio of the steered:unsteered beam is 0.41; the on/off ratio is 3.9 at the steered and 10.1 at the unsteered beam location. Beamsteering contrast and efficiency can be increased by achieving higher fill-factor in the phased array.

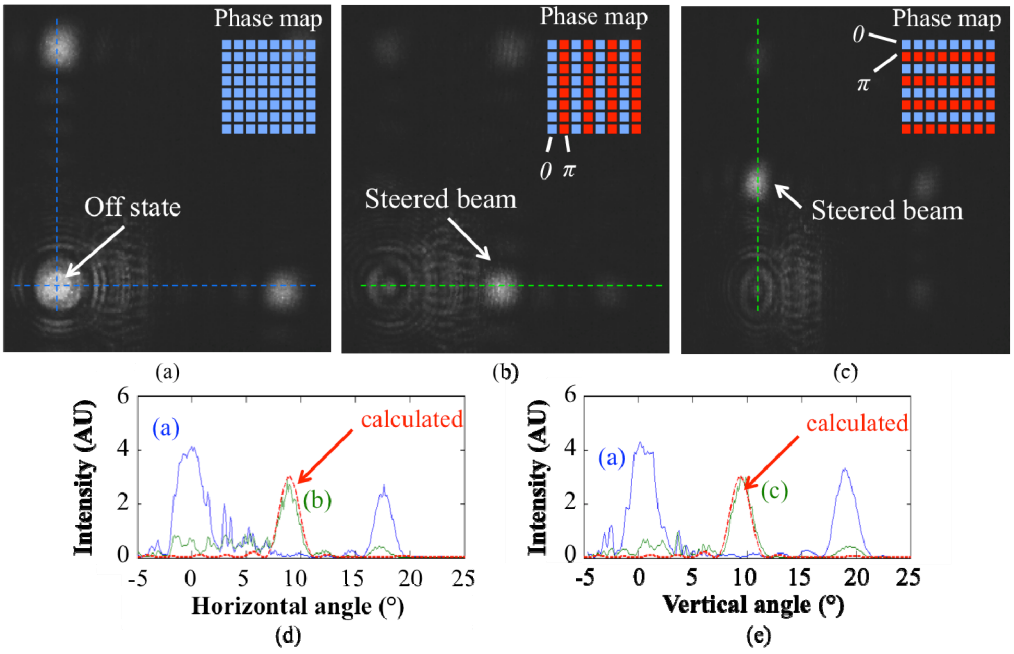

Fig. 8. Measured beamsteering in two dimensions. (a) off state, (b) beamsteering along the horizontal axis, (c) beamsteering along the vertical axis, (d, e) comparison of measured and calculated intensity along the horizontal (resp. vertical) axis.

5. Conclusions

We have fabricated an 8 × 8 phased array incorporating MEMS HCG mirrors on a SOI wafer, characterized its resonant frequency and time response, and demonstrated 1.26° beamsteering in two dimensions. The HCG is designed to have 99.9% reflectivity at a wavelength of 1550 nm and maintains such high reflection along a wider bandwidth than a DBR. Thanks to the low mass of HCGs on a SOI wafer, a fast time response is attained, on the order of microseconds. The fill-factor of the current device is 36%. High fill-factor may be prerequisite for various beamsteering applications. This can be realized by either using smaller anchor design with silicon nitride safe in HF release or designing electrical lines hidden under the HCG device layer. The single layer HCGs are resistant to thermally induced stress. This can broaden the application area of MEMS phased arrays to high energy lasers. The results support the potential of MEMS HCG phased array in realizing various beamsteering applications.

#182670 - $15.00 USD Received 2 Jan 2013; revised 8 Mar 2013; accepted 13 Mar 2013; published 10 May 2013

Acknowledgments

The authors would like to acknowledge support from the DARPA SWEEPER program (No. HR0011-10-2-0002).

#182670 - $15.00 USD Received 2 Jan 2013; revised 8 Mar 2013; accepted 13 Mar 2013; published 10 May 2013